Dye-sensitized solar cell based on nanocrystalline TiO$_2$ with 3–10 nm in diameter

Jinting Jiu · Seiji Isoda · Motonari Adachi · Hao Wang

Abstract Nanocrystalline TiO$_2$ with 3–10 nm in diameter was prepared with a surfactant-template method. Dye-sensitized solar cells were assembled using the prepared nanocrystalline TiO$_2$ with large surface area and high crystallinity, which achieved significant higher Jsc when compared to cells fabricated with bigger particles of 25 nm in diameter. In the cells with nanocrystalline TiO$_2$, the sintering temperature drastically affected the conversion performance of the cells.

1 Introduction

Dye-sensitized solar cells (DSSC) developed by Grätzel and coworkers are currently attracting widespread academic and industrial intense interest due to their high solar conversion efficiency over 10% at a very competitive cost [1–3]. The operation is driven by electron injection from photoexcited dyes into the conduction band of TiO$_2$ (anatase). Recently, many scientific groups have focused on relevant studies to verify the results, to attempt to use different possible sensitized dyes, to investigate physical properties of electrons transport, and to improve composition of electrolytes. In all those experiments, highly porous layers were commonly used as TiO$_2$ electrodes, which have been recommended already by Grätzel's group. According to this concept, various techniques have been developed to prepare the nano-porous TiO$_2$ film, which is one of the key components for high power-conversion efficiency in DSSC. Until now, however, only large diameter TiO$_2$ nanoparticles have been adopted; for example, Grätzel and coworkers used TiO$_2$ nanoparticles of 10 ~ 20 nm in diameter, which were prepared by a hydrothermal method, as an electrode for DSSC and achieved an efficiency of 10–11% [1–3]. Kambe et al. [4] synthesized single-phase anatase TiO$_2$ nanocrystals with 11–13 nm in diameter by a direct hydrolysis of titanium butoxide in an organic solvent under high pressure and high temperature (150–300 °C). The photovoltaic property of the highly transparent cell with 16 μm film thickness was concluded to be superior to that of P-25 film with 11 μm film thickness. Also Ito et al. [5] have investigated extensively the formation process and coating technique of P-25 film with the particle diameter of about 25 nm, but the conversion efficiency could not exceed 7%. Li et al. [6] prepared pure anatase type TiO$_2$ particles with the diameter of 100 nm by using titanium butoxide in butanol by a sol-gel method. However, the film electrode yielded nearly the same efficiency to that with a film electrode composed of P-25. Recently, Wang et al. [7] prepared a series of TiO$_2$ nanoparticles with the diameters of 23, 50 and 100 nm

J. Jiu (✉) · S. Isoda
The Institute for Chemical Research, Kyoto University, Uji, Kyoto 611-0011, Japan
e-mail: jiu@eels.kuicr.kyoto-u.ac.jp

M. Adachi
The International Innovation Center, Kyoto University, Yoshida-Honmachi, Sakyo, Kyoto 606-8501, Japan
e-mail: adachi@iae.kyoto-u.ac.jp

H. Wang
Department of Materials Science and Engineering, Beijing University of Technology, Chaoyang district, Beijing 100022, China

by a hydrothermal method, and reported that a high efficiency over 10% has been obtained in a mixture of these nanoparticles. These results suggest clearly that DSSC performance depends on the size and crystallinity of the TiO_2 particles and additionally the TiO_2 particles must be prepared with good dispersion. As a result, smaller particles could be expected to achieve higher conversion efficiency in the DSSC generally. So far, TiO_2 electrodes composed of nanoparticles smaller than 10 nm have not been reported in the DSSC application.

In this paper, we report successful preparation of nanocrystalline TiO_2 (N-TiO_2) electrode with diameter of 3–10 nm by a surfactant template method and discuss the influence of particle diameter, sintering temperature and film thickness on the performance of the solar cell.

2 Experimental details

The preparation of nanocrystalline TiO_2 was as follows: First 6 g of copolymer F127 (poly(ethylene oxide)$_{106}$-poly(propylene oxide)$_{70}$-poly(ethylene oxide)$_{106}$) was dissolved in distilled water by fixing the pH value with a HCl solution. And then an orange-color mixture solution of 6.8 g of TIPT (tetraisopropylorthotitanate) and 2.4 g of ACA (acetylacetone) was poured into the above F127 acid solution. The immediately formed yellow precipitation was stirred at 40 °C until a uniform transparent yellow solution was obtained. After the solution was kept at 80 °C in a closed container for over three days, a bright yellow, transparent, soft and stable TiO_2 gel was obtained. Neither separation nor supernatant could be observed even after the gel was left in the 80 °C oven over two months. For preparation of photoelectrodes, the gel was simply stirred to become a somewhat fluid solution and then one drop of the gel was spread onto a conducting glass substrate, followed by drying at 40 °C for several min and sintering at a determined temperature shortly for 10 min in an oven. After the treatment, the hot film was taken out from the oven and cooled down to about 60 °C. Further layers were coated successively on the hot film and repeated the above process until a designed thickness of N-TiO_2 films was fabricated. At last, the film was calcined for 1 h at a determined temperature. The film was soaked in a solution of N719 dye (Solaronix) for over 12 h so as to cover the TiO_2 surface with the dye. The dye-adsorbed TiO_2 electrode was assembled into a sandwich-type cell with a counter electrode (platinum-sputtered ITO glass) by clamps. The cell size of the N-TiO_2 film was 0.25 cm^2. A drop of electrolyte

solution (0.1 M LiI, 0.6 M DMPII (1,2-dimethyl-3-n-propylimidazolium iodide), 0.05 M I_2 and 0.5 M TBP (4-tert-butylpyridine) in methoxyacetonitoryl) was introduced into the clamped electrodes. The cells made of P-25, a commercial TiO_2 particle containing both anatase and rutile phases, were also prepared for comparison.

3 Results and discussion

Figure 1 shows the XRD patterns of the N-TiO_2 film calcined at different temperatures together with that of P-25 film. Peaks 2 and 3 are diffraction peaks from the substrate used. The diffraction signal assigned to the anatase (101) spacing at $2\theta = 25.3°$ (peak 1) is clearly observed in both N-TiO_2 and P-25 films. The diffraction signal at 27.5° due to the rutile phase (110) spacing is not observed in the N-TiO_2 films, different from the case of P-25 film. The intensity ratio of the diffraction peaks figures out ca. 20 % content of rutile in the P-25 film. Absence of the rutile diffraction in the N-TiO_2 films means that the sintering temperature in the film fabrication does not affect the crystalline phase itself even at a high temperature of 550 °C. The diffraction intensity slightly increases and the width of peak decreases with the calcining temperatures, suggesting the increases in crystallinity and particles size with temperatures. Furthermore, the half-height widths of the diffraction peaks of the N-TiO_2 films, which are inversely responded to sizes of particles, are much wider than that of P-25 even at high calcination temperatures. The sizes of particles calculated by the Scherrer's equation are about 3.9, 5.3 and 7.9 nm calcined at 350, 450 and 550 °C for the N-TiO_2 films respectively, and 23.0 nm for P-25 film.
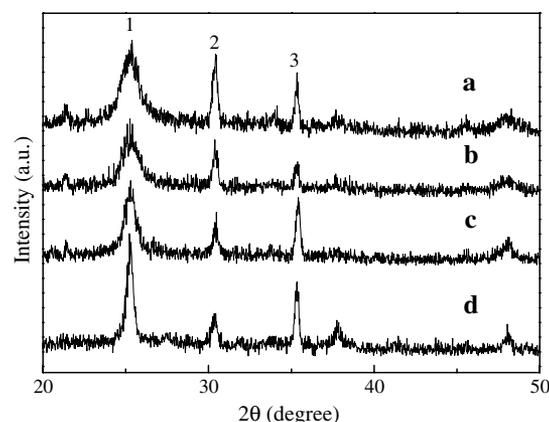
Fig. 1 X-ray diffraction spectra of TiO_2 films calcined at 350 °C (**a**), 450 °C (**b**) and 550 °C (**c**), and P-25 film (**d**)

Figure 2 shows the morphology of N-TiO$_2$ particles that were peeled off from the glass substrates with different calcined temperatures. The TEM images reveal that the N-TiO$_2$ exhibits irregular spherical shapes with a size distribution of 3–5 nm. With increasing temperature, the irregularity (deviation from spherical shape) is enhanced and evolved further into a square- or hexagonal-shape particle with high crystallinity evidenced by the clear lattice fringes and sharp crystallite edges. Furthermore, the diameter of particles is increased to 5–10 nm at 450 and 550 °C, even though much larger particles were observed occasionally at such high temperatures. This fact agrees well with that expected from XRD data. At 350 °C, the randomly packed particles show many grain boundaries among the particles, which indicates the lattice discontinuity in these parts and consequently results into distortion in carrier transport. With increasing temperature, the crystalline shape becomes clear and sharp as shown by the lattice fringes in the TEM images (Fig. 2b and 2c), suggesting that the crystallinity of particles is improved and enhanced with the heat energy. On the other hand, it should be noted that the necking regions (typically shown in Fig. 2b with white ellipses) between the particles are observed at higher temperature treatments, which is expected to be advantageous for the transport of electrons in the skeleton comparing films packed simply with single particles. The necking regions are developed with the heat energy presumably by the heat-melting growth or coalescence between particles, which is also evidenced by the formation of larger particles observed in TEM images with increasing temperature.

The effect of sintering temperature on the performance of cell was examined. Figure 3 shows the photocurrent-voltage curves of N-TiO$_2$ films calcined at 350, 450 and 550 °C. Clearly the higher temperature sintering induces higher photocurrent and higher conversion efficiency of light-to-electricity. An important factor to improve cell performance is the amounts of dye adsorbed, but the amounts in these films were decreased from 1.25, 1.07 to 0.89 × 10^{-7} mol/cm^2 with

the temperatures. However, one needs to consider here the actual thickness of films in the cells, which was different from cell to cell in the present study although these films were fabricated similarly with the five-times coating by doctor blade method. Before calcination, every coating can generate one pre-film with a thickness of about 30–40 μm, but the thickness of film shrunk down to 6.7, 5.5 and 4.3 μm when treated at 350, 450 and 550 °C, respectively. Therefore, it can be concluded that the resulted thickness of film for every coating is about 1.34, 1.1 and 0.86 μm with increasing sintering temperature. When considering that the thinner film always adsorbs less dye molecules, the amounts of dye might decrease with calcinations temperature as described above. The decrease of adsorbed dye can also relate to the decrease in the surface area of films owing to the necking parts between particles as well as larger particle size, as demonstrated with the analysis of nitrogen isotherm and TEM observation. When the sintering temperature is increased from 350 °C to 550 °C, the surface area was drastically decreased from 151, 106 to 78 m^2/g, respectively, as measured by nitrogen isotherm. Hence, the observed high efficiency at high sintering temperature indicates that the film structure, not the thickness, may play a key role in DSSC. Zukalova et al. [8] have already reported that the performance of DSSC fabricated with organized mesoporous TiO$_2$ film is expected to be improved, when the crystallinity of the mesoporous TiO$_2$ skeleton is enhanced by high sintering temperature. In our case, the increasing temperature leads to the formation of highly crystallized film composed of coalesced nanocrystals as shown in TEM and XRD measurements, which improves the structure of film and enhances the interconnection between particles, resulting in the swift diffusion of electrolyte and better transport of electrons in the film. Furthermore, the high temperature treatment also contributes to the decreased amount of impurity; for example, possible carbon residues remained after copolymer F127 was burned. Such impurity generally makes worse the crystallinity of oxide and generates trapping sites for the electrons.

Fig. 2 TEM images of TiO$_2$ particles peeled from calcined films at 350 °C (**a**), 450 °C (**b**) and 550 °C (**c**)
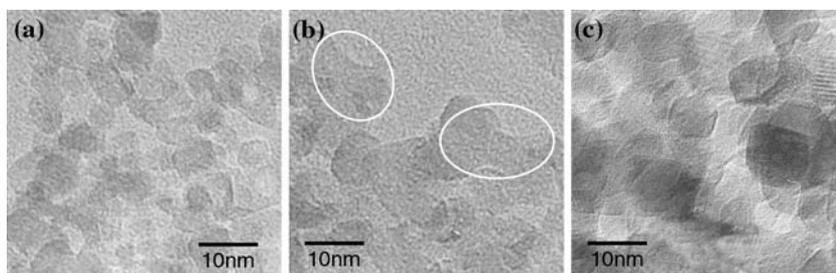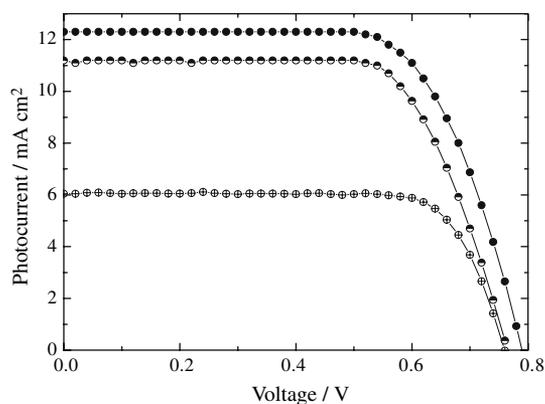
Fig. 3 Photocurrent-voltage curves of N-TiO$_2$ films calcined at 350 °C (⊕), 450 °C (◓) and 550 °C (●)

In particular it should be mentioned here that the N-TiO$_2$ films composed of very small particles are fully transparent irrespective to the thickness and sintering temperature, while P-25 film is translucent or opaque with the thickness. Hence the scattering of light due to large particles does not contribute to the photovoltaic response of the N-TiO$_2$ film systems compared to the system consisting of P-25 film. The IPCE spectra (Fig. 4) indicate the effect due to scattering of light. In opaque P-25 films with the thickness of 10.8 μm, the IPCE values are drastically increased in the long wavelength region (650–750 nm), which is generally attributed to the light scattering effect in the region with such large particles because of the longer path-depth of the long wavelength light. Contrarily, in the same long wavelength region, the other transparent N-TiO$_2$ and P-25 films show lower IPCE values, suggesting the inefficient light scattering contribution. On the other hand, in the short wavelength region (400–600 nm), high IPCE values are always achieved in the N-TiO$_2$ film especially for thinner films when
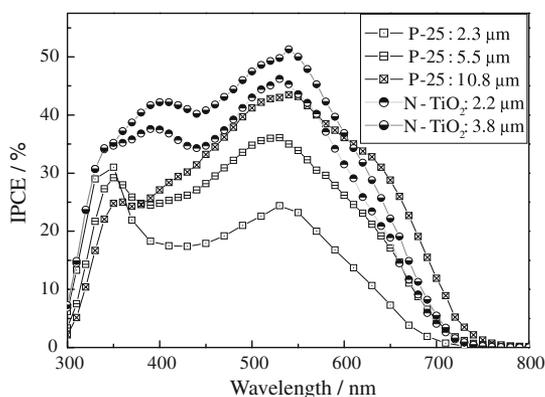
Fig. 4 Photocurrent action spectra of N-TiO$_2$ and P-25 electrodes with different thickness of films

comparing that of P-25 film with similar thickness. The difference could be explained by the amount of adsorbed dye molecules compared with P-25 film, since the amount of dye adsorbed on the N-TiO$_2$ film is more than twice as much as that on the P-25 film at the same thickness. Therefore, we believe that the high efficiency of N-TiO$_2$ is not resulted from the stronger light scattering but from the high crystallinity with small amount of impurity, the large surface area with much more amount of adsorbed dye and optimized film structure. The other important factor is the crystal characteristics. Generally, lattice imperfections in crystal such as vacancies, and lattice dislocations interfere with electron transport in semiconducting materials. Considering that P-25 is a mixture of ca. 80% anatase and ca. 20% rutile nanocrystallites (Fig. 1), the high photocurrent generation in the N-TiO$_2$ film with good crystallinity is originated from the fact that the transport of photo-injected electrons should become effective in the single-phase anatase TiO$_2$ film agglomeration.

With the present N-TiO$_2$ film, 7.54% conversion efficiency, the open circuit photovoltage of 759 mV, the short circuit photocurrent of 13.5 mA/cm^2 and the fill factor 0.748 have been obtained at the thickness of 6 μm. However, higher efficiency is difficult to be achieved with only the N-TiO$_2$ film composed of very small nanoparticles and the sensitized dye of N719 due to the low light harvest in the long wavelength region. As it has been suggested, the tuning of TiO$_2$ photo-electrode morphology is essential and necessary for higher efficiency [7] such as multilayer cell made of nanoparticle layers and light-scattering particle layers on conductive glass substrates in a desired sequence and thickness. The optimized film morphology composed of the small nanoparticles and large scattering particles will be studied in the future work. In the present study we demonstrate that the small nanoparticles, N-TiO$_2$ film, achieve a significant high efficiency and also improve the contact between the substrate glass and TiO$_2$ film as well as the interconnection among the particles due to their small size by directly deposition on the substrate from the gel state.

4 Summary

The TiO$_2$ gel prepared with copolymer F127 template can be used to form high performance N-TiO$_2$ film with size of 3–10 nm and high surface area. The performance of the transparent film electrode is affected by the sintering temperature which improves the crystallinity, crystal phase, crystal size and surface

area of the particles and film structure. A high efficiency over 7.5% is achieved with only the small nanoparticles.

References

1. B. O'Regant, M. Grätzel, Nature **353** 737 (1991)
2. M. Grätzel, Nature **414** 338 (2001)
3. M. Grätzel, J. Photochem. Photobiol. A: Chem, **164** 3 (2004)
4. S. Kambe, K. Murakoshi, T. Kitamura, Y. Wada, S. Yanagida, H. Kominami, Y. Kera, Sol. Energy Mater. Sol. Cells **61** 427 (2000)
5. S. Itoa, T. Kitamurab, Y. Wada, S. Yanagida, Sol. Energy Mater. Sol. Cells **76** 3 (2003)
6. Y. Li, J. Hagen, W. Schaffrath, P. Otschik, D. Haarer, Sol. Energy Mater. Sol. Cells **56** 167 (1999)
7. Z. Wang, H. Kawauchi, T. Kashima, H. Arakawa, Coord. Chem. Rev. **248** 1381 (2004)
8. M. Zukalova, A. Zukal, L. Kavan, M.K. Nazeeruddin, P. Liska, M. Gratzel, Nano. Lett. **5** 1789 (2005)